Inorganic Chemistry

Article

pubs.acs.org/IC

Relationships between Electron Density and Magnetic Properties in Water-Bridged Dimetal Complexes

Jacob Overgaard,*[,†] James P. S. Walsh,[⊥] Venkatesha R. Hathwar,[†] Mads R. V. Jørgensen,[†,‡] Christina Hoffman,[‡] Jamie A. Platts,[§] Ross Piltz,[∥] and Richard E. P. Winpenny[⊥]

[†]Department of Chemistry, Center for Materials Crystallography, Aarhus University, DK-8000 Aarhus C, Denmark

[‡]Chemical and Engineering Materials Division, Oak Ridge National Laboratory, PO Box 2008 - MS 6475, Oak Ridge, Tennessee 37831, United States

[§]School of Chemistry, Cardiff University, Park Place, Cardiff, CF10 3AT, U.K.

[∥]Bragg Institute, ANSTO, Locked Bag 2001, Kirrawee DC, NSW 2232, Australia

[⊥]School of Chemistry and Photon Science Institute, The University of Manchester, Oxford Road, Manchester M13 9PL, U.K.

Supporting Information

ABSTRACT: The electron densities in two analogous dimetallic transition metal compounds, namely, $[M_2(\mu\text{-}OH_2)(^t\text{BuCOO})_4(^t\text{BuCOOH})_2(C_5H_5N)_2]$ (M = Co(**1**), Ni(**2**)), were determined from combined X-ray and neutron single-crystal diffraction at 100 K. Excellent correspondence between the thermal parameters from X- and N-derived atomic displacement parameters is found, indicating high-quality X-ray data and a successful separation of thermal and electronic effects. Topological analysis of electron densities derived from high-resolution X-ray diffraction, as well as density functional theory calculations, shows no direct metal−metal bonding in either compound, while the total energy density at the bond critical points suggests stronger metal−oxygen interactions for the Ni system, in correspondence with its shorter bond distances. The analysis also allows for estimation of the relative strength of binding of terminal and bridging ligands to the metals, showing that the bridging water molecule is more strongly bound than terminal carboxylic acid, but less so than bridging carboxylates. Recently, modeling of magnetic and spectroscopic data in both of these systems has shown weak ferromagnetic interactions between the metal atoms. Factors related to large zero-field splitting effects complicate the magnetic analysis in both compounds, albeit to a much greater degree in **1**. The current results support the conclusion drawn from previous magnetic and spectroscopic measurements that there is no appreciable direct communication between metal centers.

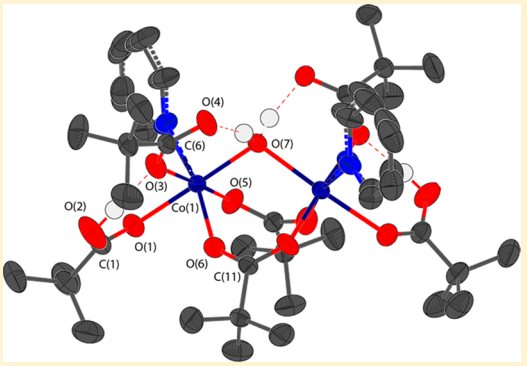

INTRODUCTION

Dimetallic clusters containing ions bridged by oxo/hydroxo/water moieties—in particular those incorporating iron and manganese as the metals—have been studied for decades, primarily as mimics of the active sites in many important enzymes.[1] In addition to their biological relevance, however, they are also studied for their magnetic properties.[2] In this latter example, the dimer compounds are of interest because they allow magnetochemists to examine individually the same exchange pathways found in larger multinuclear compounds, without the inherent complications that arise when having to treat a large number of ions simultaneously. Oxygen-bridged dimers are particularly studied for this purpose, since many single-molecule magnets (SMMs) utilize such species as bridging ligands, the archetypal Mn_{12} cluster being a prime example.[3]

The vast majority of intramolecular exchange interactions are antiferromagnetic (AFM), which makes examples of ferromagnetic (FM) interactions particularly interesting. Indeed, the ability to predict the factors necessary for FM interactions would be very useful for magnetochemists aiming to maximize the ground-state total spin in new molecules, since this is an important consideration when targeting SMM behavior.[4]

A unique class of so-called "water-bridged" dimer compounds (containing either Co(II) or Ni(II) centers bridged by two carboxylates and a water molecule, see Scheme 1) have recently been shown to exhibit contrasting exchange interactions (AFM/FM) after very small chemical and structural changes,[2] but the reasons for the switch in behavior are not well understood. While the M−O−M angle seems to be important,[2a] as is well-known to be the case in spin-only dimers,[5] the observed trends are qualitative at best, and offer little insight into the cause of the change in behavior. This is due largely to the enormous complexity involved in modeling magnetic/spectroscopic data in compounds wherein spin−orbit

Received: June 22, 2014
Published: October 20, 2014

   dx.doi.org/10.1021/ic501411w | *Inorg. Chem.* 2014, 53, 11531−11539

Scheme 1. Schematic of the Chemical Bonding Present in Compounds 1 and 2

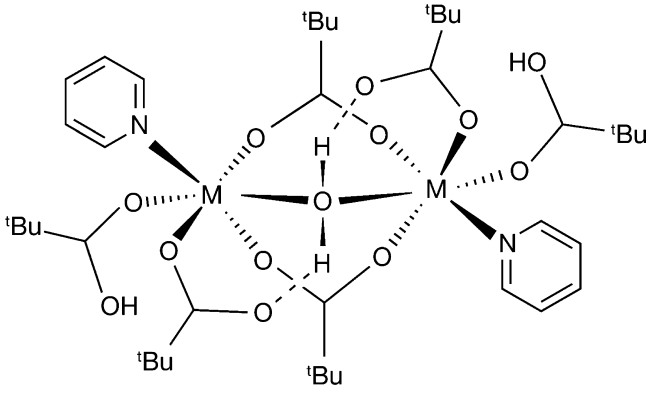

coupling is significant (thus rendering a spin-only treatment completely inappropriate). Elucidation of the underlying cause of the switch in the sign of the exchange will therefore almost certainly rely on the *direct* measurement of the electronic structure involved in the exchange.

The dimer systems that are the focus of this work are two compounds from the family of water-bridged dimers mentioned above. In these systems, the metal−metal distance is sufficiently large that no direct bonding interaction is expected to take place. Instead, the communication likely occurs through superexchange pathways between the spin centers—in this case along the bonds of the bridging water and/or carboxylates—rendering the nature and strength of the chemical bonding in these intervening bonds an important factor to consider in our investigation of the magnetic coupling. The electron density distribution (ED) of a system contains exactly this information about the chemical bonding, with the added benefit that it can be studied experimentally by analysis of high-resolution single-crystal X-ray diffraction data.[6]

In this study we therefore present an analysis of the experimental and theoretical EDs in two isomorphous molecular systems having the formula $[M_2(\mu\text{-}OH_2)(^t\text{BuCOO})_4(^t\text{BuCOOH})_2(C_5H_5N)_2]$ and with M = Co (**1**), Ni (**2**). The ED enables a quantitative analysis of the chemical bonding using the partitioning of space derived from the theory of Atoms in Molecules pioneered by Richard Bader,[7] and will be supplemented here by results obtained by theoretical methods.

Compounds **1** and **2** are isomorphous in terms of crystal structure, differing only in the identity of the metal centers. Compound **1** contains Co(II) ions in an approximately octahedral environment and thus exhibits electronic effects related to a very strong first-order orbital angular momentum. The nearly octahedral Ni(II) ions in **2** are not affected in the first-order by spin−orbit coupling, but exhibit a significant zero-field splitting (ZFS) due to mixing of excited states with the ground state. Although the ferromagnetic interaction is evidenced by an upturn in the molar magnetic susceptibility at base temperatures in **1**, the interaction in **2** is heavily masked by the significant ZFS. Indeed, the downturn at lower temperatures in the susceptibility of **2** has led to the interpretation that the exchange interaction in this compound is strongly antiferromagnetic,[8] but recent work by some of the authors has revealed that the interaction is actually extremely weak, and likely ferromagnetic.[9]

The molecules studied here belong to a larger group of systems with the general formula $[M_2(\mu\text{-}OH_2)(^t\text{BuCOO})_4(L)_2(L')_2]$, where L and L′ are pivalic acid molecules in the parent compound and are readily substituted by N-donor ligands (such as pyridine and derivatives thereof). The majority of the compounds in this family exhibit singlet ground states due to AFM intramolecular coupling, with **1** and **2** being two of the few exceptions to this trend.

The pivotal point of this paper will be the study of the bonding interactions in the central regions of these compounds, which are expected to be heavily influential in determining the nature of the exchange interaction. Given the fact that only small changes to the molecular geometries are required to fundamentally impact the magnetic coupling in these systems,[9] it is likely that any changes to the density and derived properties will be similarly small. Since these compounds crystallize well and form large crystals, the current study will include anisotropic thermal parameters for hydrogen atoms derived from neutron single crystal diffraction, which has previously been shown to have a significant influence even on atoms not directly bonded to hydrogen.[10]

EXPERIMENTAL SECTION

Synthetic Procedure. Compounds **1** and **2** were prepared following literature procedures.[9,11] All chemicals were purchased from Sigma-Aldrich and were used without further purification.

Neutron Data Collection. *Compound 1.* Data collection was performed using the Laue Single Crystal instrument KOALA at the OPAL reactor of the Australian Nuclear Science and Technology Organisation.[12] A crystal of approximate dimensions 1.4 × 0.7 × 0.6 mm was wrapped in aluminum foil and then adhered to an aluminum sample pin using a thin layer of perfluorinated grease. The sample was cooled using the standard KOALA helium refrigerator. Data sets were collected at 100 K using a total of 17 exposures with duration of 1 h. The data set was processed using the LaueG software suite that incorporates a modified version of ARGONNE_BOXES for peak integration,[13] and the Laue4 program for wavelength normalization, scaling, efficiency, secondary extinction, and harmonic overlap corrections.[14] Of the total number of spots integrated, approximately 27% were rejected prior to normalization for being outside the wavelength limits of 0.8 and 1.8 Å, for being expected to have strong harmonic overlap, or for having a redundancy of only 1. The intensity uncertainties from the integration process were increased to (1.3 δ(I) + 0.02 I) as a result of a statistical analysis of the merging process. Intensities were merged over repeated measurements, equivalent reflections, and Friedel pairs, resulting in 6779 unique intensities with an R_{merge} of 10.8%. A correction for sample absorption was not performed due to the small size of the crystal and the wavelength limits used, and because the wavelength normalization process partially corrects for sample absorption. The disorder of the pyridine ring resulted in a distribution of 74:26.

Compound 2. A crystal with dimensions of approximately 1.0 × 1.0 × 1.3 mm^3 was mounted on the end of a thin-walled polyamide tube using cyanoacrylate glue to minimize incoherent scattering from the sample mount. The sample was placed on the goniometer of the TOPAZ single-crystal time-of-flight Laue diffractometer at the Spallation Neutron Source, Oak Ridge National Laboratory.[15] The sample was cooled from 295 to 100 K at 180 K/hour using an Oxford Cryosystems Cryostream Plus liquid nitrogen cooling device.[16]

TOPAZ utilizes 13 Anger cameras, each with an active area of ca. 15 × 15 cm^2 arranged on a nearly spherical detector array tank around the sample. The total flight path of 18.4 m and the 60 Hz repetition rate provides a usable wavelength bandwidth of 3.6 Å.

Data was collected using 16 settings calculated to maximize the completeness of the data using the program CrystalPlan.[17] The data were indexed and integrated using ellipsoids in q-space[18] as implemented in the Mantid program.[19]

dx.doi.org/10.1021/ic501411w | Inorg. Chem. 2014, 53, 11531−11539

Table 1. Crystallographic Details from the Multipole Refinement Using X-ray Data

	1	2
empirical formula	$Co_2C_{40}H_{68}N_2O_{13}$	$Ni_2C_{40}H_{68}N_2O_{13}$
formula weight, g mol^{-1}	902.82	902.39
crystal size (mm)	0.20 × 0.27 × 0.35	0.20 × 0.24 × 0.25
crystal system	monoclinic	monoclinic
space group	$C2/c$	$C2/c$
λ, Å	0.7107	0.7107
a, Å	24.6879(1)	24.5019(2)
b, Å	19.4565(1)	19.4650(1)
c, Å	9.753 36(4)	9.7790(1)
β, deg	96.6302(4)	96.499(1)
V, Å^3	4653.61(4)	4633.92(7)
Z	4	4
$F(000)$	1920	1928
T, K	90	100
ρ, g cm^{-3}	1.289	1.316
μ, mm^{-1}	0.772	0.872
T_{max}, T_{min}	1.196, 0.934	1.000, 0.836
$\sin(\theta)/\lambda_{max}$, Å^{-1}	1.1	1.1
N_{meas}, N_{uniq}	345 652, 32 245 (22 187 to 1.1 and $I > 2\sigma(I)$)	247 786, 25 844 (21 549 $I > 2\sigma(I)$)
redundancy	9.8	9.6
completeness	0.997	1.000
R_{int}	0.0488	0.0365
N_{obs}, N_{var}, ($I > 2\sigma(I)$)	22 187, 712	21 549, 730
$R_w(F^2)$, ($I > 2\sigma(I)$)	0.042	0.054
$R(F)$, $R(F^2)$, all data	0.025, 0.024	0.045, 0.027
goodness of fit	1.07	1.412

A total of 130 179 predicted reflections were integrated. The data were corrected for absorption and scaled to the incident spectrum using the program ANVRED2.[20] During this step all data with $I/\sigma(I) < 1$ and reflections near the edges of the detectors were discarded. This led to 37 790 reflections, which were loaded into the refinement program GSAS.[21] The coverage, excluding the edges of the detectors, is 86.3% up to a maximal resolution of 0.5 Å. The starting coordinates were taken from an X-ray diffraction model. After co-refining positions and anisotropic parameters for all atoms plus a secondary type I extinction model with a Lorentzian spread, 4159 outliers were removed from the data using $((F_o^2)/(F_c^2)) > 10$, $((F_c^2)/(F_o^2)) > 10$, and $|F_o^2 - F_c^2|/\sigma(F_o^2) > 10$. In addition to these outliers, 15 569 reflections with $I/\sigma(I) < 2$ were removed, leaving a total of 18 062 reflections for the refinement. Removing these outliers and weak reflections did not change the parameters significantly but naturally diminished the residual.

The structure was refined in the GSAS program with anisotropic displacement parameters (ADPs) for all atoms including hydrogens. Detailed evaluation of the ADPs of the outer three carbon and hydrogen atoms on the pyridine ring in the structure reveals very large displacement ellipsoids, indicating that the whole pyridine moiety is disordered. The disorder refinement was not stable in GSAS as the geometries of the disordered ring and ADPs were unphysical. Hence, the reflections corrected for extinction based on the GSAS model were extracted. The disordered model was refined in SHELXL[22] using Olex2.[23] The ADPs of the pairs of disordered atoms in the pyridine ring were constrained to be identical. The final refinement resulted in occupancy of the two parts in the ratio of 76:24, which is almost identical to the X-ray disorder model (*vide infra*). The obtained X−H distances and scaled ADPs of hydrogen atoms were incorporated in the XD model for the electron density evaluation.

X-ray Data Collection and Structure Refinement. *Compound 1.* For compounds with Co and Ni, suitably sized and shaped single crystals were selected and mounted using Paratone-N oil on the tip of a glass pin and attached to a goniometer-head. This was fixed to the goniometer of an Agilent Technologies Supernova diffractometer and centered in the X-ray beam from a microfocus Mo source. The crystal was cooled to 90 K with liquid N_2 using an Oxford Cryosystems Cryostream 700 device.[16] The data collection time was optimized to reach completeness to a resolution of 0.47 Å while maximizing the redundancy. The exposure time was fixed at 10 s for the low-order region ($2\theta \approx 40°$) and 120 s for the high-order data ($2\theta \approx 90°$). The data set was integrated and corrected for Lorentz and polarization using the CrysalisPRO software,[24] and face-indexed absorption correction was performed before additional corrections such as frame scale factors were carried out with ABSPACK. The resulting intensities were merged in Laue group 2/m in the program SORTAV.[25] The maximum resolution reached in the data collection was 1.22 Å^{-1}; however, the majority of reflections in the outer shell were insignificant and therefore omitted from the final data set. Additional numerical details are tabulated in Table 1.

The two crystal structures (**1** and **2**) are isomorphs and crystallize in the monoclinic space group $C2/c$. The structures were solved independently by direct methods (SHELXS[22]) before the subsequent refinement of an independent atom model (IAM) using Olex2[23] and SHELXL.[22] All hydrogen atoms were located in difference Fourier analysis. The asymmetric unit contains only half of the molecule, with a 2-fold rotation axis bisecting it through the bridging oxygen atom in the water molecule. An ORTEP[26] drawing of the Co structure (**1**) is shown in Figure 1. The original publication of the crystal structure based on normal resolution data (ca. 0.75 Å) did not reveal any disorder in the structure. However, with access to high-resolution data it becomes immediately clear that the three outer carbon atoms of the pyridine ring in particular exhibit large anisotropic thermal ellipsoids within the ring plane, suggesting that this moiety is in fact disordered. The disorder is such that the pyridine ligand, acting as a rigid group, librates around an axis that is perpendicular to the molecular plane, and intersects the plane close to the N atom. The effect is therefore much larger on the peripheral three C atoms being furthest away from the axis and smaller on the three atoms closer to the rotation axis. Nevertheless, for both compound **1** and **2** the best models included disorder on all six atomic positions (*vide infra*). The ADPs of the pairs of disordered atoms were constrained to be identical. In compound **1**, the relative occupancy of the two parts refined to 85:15. These values

dx.doi.org/10.1021/ic501411w | Inorg. Chem. 2014, 53, 11531−11539

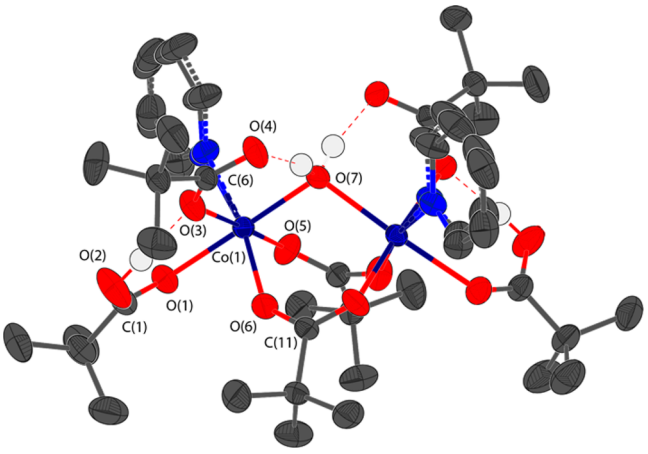

Figure 1. ORTEP[26] drawing of **1** showing 90% probability ellipsoids. All hydrogen atoms bonded to carbon were omitted for clarity.

deviate from the disorder distribution found at 100 K in the neutron diffraction data of **1** (74:26). The reason for this discrepancy is that the X-ray data were collected at 90 K, exemplifying the dynamic behavior of the disorder.

Compound **2**. A good quality single crystal of suitable size (0.20 × 0.24 × 0.25 mm^3) of **2** was selected for the high-resolution X-ray data collection at 100 K. The experimental setup and data collection procedures were kept similar to those described above for compound **1**. Complete data out to d = 0.45 Å was collected using two different 2θ-settings. The exposure times were 15 and 150 s for the low-order region ($2\theta \approx 40°$) and the high-order data ($2\theta \approx 90°$), respectively. The data reduction steps were identical to those for compound **1**. As mentioned above, disorder of the entire pyridine ring was also apparent for compound **2**, highlighting the structural similarity between the two compounds. The occupancy of the two disordered parts was found to be 76:24 in compound **2**. This ratio is slightly more even than the distribution obtained in the X-ray structure of **1** measured at the lower temperature of 90 K, but indistinguishable from the values found from the neutron data for **1**, which was measured at the same temperature (100 K). This supports the idea that the distribution of the disorder is dictated by temperature and that it is virtually unaffected by the identity of the metal.

Multipole Modeling. *Compound* **1**. The IAM parameter files were used as input for subsequent multipole modeling in the program XD,[27] which uses the Hansen−Coppens formalism.[28] A number of models were tested to optimize the fit to the data, including different scattering factors (ionic or neutral) for the central metal atom. The final model used an ionic scattering factor for Co from the SCM database,[29] and the model included up to hexadecapoles for the nondisordered non-hydrogen atoms, while the C and N atoms in the disordered part are only described using octupoles. The aspherical density of H atoms is described by bond-directed dipoles and quadrupoles. The κ-parameters used to scale the radial functions were fixed to identical values for similar atom types, that is, one for Co, one for N, two for O (bridging O7 is different), three for C (carboxylate, sp^3 and pyridine), and one for H.

The initial high-order refinement fixed the atomic positions and thermal parameters for non-H atoms, while the anisotropic thermal parameters for H were scaled and imported from the neutron model (*vide infra*). The X−H bond distances were fixed to values from the

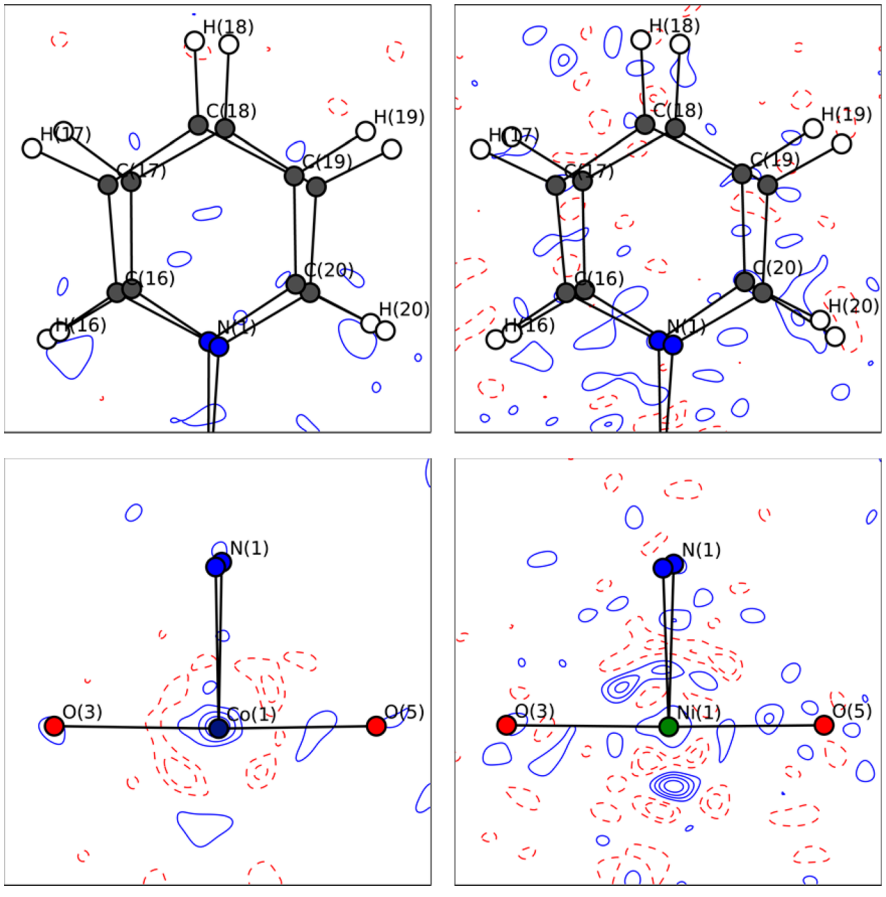

Figure 2. Residual density maps of selected planes for **1** (left) and **2** (right). The upper row shows the pyridine ring plane, while the lower row shows the residual in a plane defined by M−N1−O5. Solid lines indicate positive values and negative values are shown using dashed lines with contour intervals of 0.1 e $Å^{-3}$.

dx.doi.org/10.1021/ic501411w | *Inorg. Chem.* 2014, 53, 11531−11539

neutron model by moving the H atom along its bonded atom when the position of this atom is refined.

The Hirshfeld rigid bond test is clearly fulfilled in the final run,[30] with an average of 2.9×10^{-4} Å^2 for the 22 bonds in the asymmetric unit, neglecting the disordered part. The extremes of the residual density range from −0.30 to +0.43 eÅ^{-3} using all data. Two residual density maps, one of the disordered pyridine ring and one including Co are shown in Figure 2. The residual density analysis in the form of a fractal dimension plot,[31] which has been shown to be a valuable tool in diagnosing data sets for systematic errors, as well as other important uses,[32] indicates an excess of positive residual density, which may potentially bias the scale factor during refinement.

Figure 2 indicates that there may still be a minute amount of unmodeled disorder in the pyridine ring as well as some problems related to the core region of the Co atom. However, introducing a more complex disorder model involving three parts for the pyridine is not feasible, considering the remaining low residual density. The only method to efficiently remove the disorder is instead by lowering the temperature even further. The latter issue with the core region of Co may be related to the necessary introduction of an extended Hansen−Coppens model, which in this case primarily means refining an isotropic scaling of the radial dependency of the core electrons.[33] The model on which Figure 2 is based already includes this additional flexibility without completely removing the residual. It was decided to split the core in two parts, an inner part consisting of the K and L shells, which was slightly contracted ($\kappa = 1.0146(5)$), and an outer part consisting of the 3s and 3p electrons, which was contracted ($\kappa = 0.9968(5)$). Some of us have previously shown the dramatic consequences that an inaccurate description of the core region may have on the valence region;[34] however, in the present case we remain confident that the model provides an accurate description of the valence density since numerous more advanced models have been tried with no improvement to the residual.

Compound **2**. The nonspherical features of the electron density in compound **2** were modeled using the methodology described above for compound **1**. Identical local coordinate systems, chemical constraints, and values of κ' and κ'' were used to enable a direct comparison of the multipole models of the two compounds. The X−H distances and scaled ADPs of hydrogen atoms were obtained from neutron experiments (*vide infra*). After testing several XD models, it was observed that the neutral scattering factor for the atom Ni from the SCM database resulted in a better final model. In addition, the radial function describing the valence deformation density for the Ni atom was derived from the mixed 3d and 4s Slater functions. In this model, the 4s electrons were treated as a separate valence shell (P_{00}). This type of radial function was found to provide smaller residual densities around the Ni atom in compound **2** (see Figure 2). Similar residual density features around a Ni atom have recently been observed in the literature.[35]

The Hirshfeld rigid bond test[30] was fulfilled by all non-hydrogen bonds in the asymmetric unit of **2**, neglecting the disordered part of the molecule. The maximum deviation was found to be 11×10^{-4} Å^2 for the C1−O1 bond. The residual density ranges from −0.28 to +0.38 e Å^{-3}, and the highest residual density peak is observed at a distance of 1.3 Å from O1, not corresponding to bonding features; it remained in that position irrespective of the data reduction protocol used. It is important to emphasize that the presence of this feature does not influence any of the derived properties from the electron density model. As for **1**, the disorder in the aromatic group results in the broad shoulder in the residual density analysis.

Comparison of X and N adps. For both compounds **1** and **2**, the single-crystal neutron data enabled a comparison of anisotropic thermal parameters using the program UIJXN.[36] The models used in the comparisons were high-angle data refinements of an IAM model and the final neutron model, including the disorder in the pyridine ring. Recently, single-crystal neutron data collected at TOPAZ have been shown to be highly accurate and able to provide anisotropic thermal parameters for hydrogen atoms superior to other approaches.[37] Table 2 shows the comparison results.

Table 2. Key Numbers from the Comparison of X-ray and Neutron (N) Derived Thermal Parameters for the Heavy Atoms[a]

	$\langle \Delta U \rangle$	$\langle U_{ii}X/U_{ii}N \rangle$	$\langle [\Delta U/\Sigma(\Delta U)]^2 \rangle^{1/2}$
1	0.001 43(127)	0.952(145)	2.12
2	0.001 02(102)	0.971(64)	1.78

[a]Disordered atoms have not been included in the comparison.

The temperatures used in the X-ray and neutron-diffraction experiments differ by 10 K for **1**. It was therefore also anticipated that the ratio of $\langle U,X/U,N \rangle$ would decrease, as observed. The agreement between X-ray and neutron ADP values is rather good for both compounds, especially considering the temperature offset, the size and flexibility of the molecules, and the absolute temperature, and compares well with other literature values.[10b] It thus seems justified to extract scaled hydrogen atom anisotropic ADP values for subsequent electron-density modeling, as already alluded to in the above description.

Theoretical Calculations. Density functional theory (DFT) calculations were performed using the B3LYP hybrid functional[38] on truncated versions of **1** and **2** that were constructed by manually altering *tert*-butyl groups into methyl groups, retaining the experimental C−C distance. Electron densities for the ground-state spin multiplicities indicated by experiment (septet for **1** and singlet for **2**) were then recalculated using a basis set consisting of 6-31G* on all light atoms, and a Stuttgart−Dresden basis set and ECP on the metals.[39] The stability of the resulting solutions was tested, and in both cases lower-energy solutions than produced by the default SCF procedure were identified: data reported below corresponds to the lower-energy solutions, unless otherwise stated. The unrestricted septet calculation showed no evidence of spin contamination, with the calculated value of S^2 within 1% of the idealized one. QTAIM analysis[7] of these theoretical densities was then carried out using the AIMAll package.[40]

RESULTS AND DISCUSSION

Magneto-structural studies carried out on spin-only systems are often able to relate the exchange parameter J to structural parameters, such as the intermetal distance or the angle formed by the metals and a bridging moiety.[5] These structural parameters are then usually considered within the context of orbital overlap to give an intuitive understanding of the influence of geometry on magnetic communication. In systems that cannot be described purely as spin-only, the spatial components of the orbitals are not as well-defined, and comparable models are therefore much rarer.

In a recent study that involved compound **2** along with four other members of the water-bridged nickel(II) dimer family, high-field EPR was modeled in conjunction with magnetic data to elucidate exchange interactions that are otherwise hidden beneath dominating effects from significant ZFS.[9] The results of this study seem to suggest that the M−O−M angle is important, with smaller angles giving rise to an FM interaction and larger angles resulting in an AFM interaction.

A similar study by the same group was carried out on two compounds from the cobalt(II) family (compound **1** and its parent compound, $[Co_2(\mu\text{-}OH_2)(^t\text{BuCOO})_4(^t\text{BuCOOH})_4]$).[41] In this study, inelastic neutron scattering was used to determine the exchange interactions, which when combined with *ab initio* calculations enabled good fits to high-field EPR data. The M−O−M angle again seems important, with the smaller angle of 108.4(1)° giving an FM interaction, in contrast to the AFM interaction for the larger angle of 110.2(1)°.

dx.doi.org/10.1021/ic501411w | *Inorg. Chem.* 2014, 53, 11531−11539

Table 3. Electron Density and Related Properties of Selected Bond Critical Points, as well as the M···M Midpoint, for Compounds 1 and 2[a]

		R_{ij}	ρ_{bcp}	$\nabla^2\rho_{bcp}$	$d_{1\text{-bcp}}$	$d_{2\text{-bcp}}$	V	H	DI
Co−O7	exp	2.166	0.346	6.82	1.080	1.086	−0.064	0.003	
	theo		0.317	7.04	1.048	1.120	−0.061	0.006	0.280
Co−O1	exp	2.197	0.294	6.00	1.106	1.090	−0.052	0.005	
	theo		0.284	6.23	1.062	1.137	−0.052	0.006	0.241
Co−O3	exp	2.117	0.330	7.48	1.047	1.071	−0.063	0.007	
	theo		0.362	7.87	1.026	1.092	−0.070	0.006	0.308
Co−O5	exp	2.030	0.419	9.76	1.009	1.021	−0.090	0.006	
	theo		0.449	10.40	0.988	1.044	−0.096	0.006	0.373
Co−O6	exp	2.028	0.447	10.01	1.014	1.015	−0.097	0.003	
	theo		0.440	10.58	0.988	1.040	−0.096	0.007	0.311
Co···Co	expt	3.505	0.020	0.40	1.855	1.855	−0.012	0.008	
	theo		0.107	1.23			−0.079	0.003	0.005
Ni−O7	exp	2.107	0.486	7.28	1.052	1.055	−0.102	−0.013	
	theo		0.364	8.33	1.055	1.051	−0.074	0.006	0.315
Ni−O1	exp	2.146	0.418	6.29	1.078	1.068	−0.082	−0.009	
	theo		0.316	7.08	1.078	1.068	−0.061	0.006	0.260
Ni−O3	exp	2.088	0.466	7.11	1.042	1.046	−0.096	−0.011	
	theo		0.369	8.43	1.004	1.086	−0.075	0.006	0.333
Ni−O5	exp	2.001	0.547	8.84	0.996	1.005	−0.124	−0.016	
	theo		0.459	11.05	0.967	1.036	−0.102	0.006	0.404
Ni−O6	exp	2.002	0.553	9.01	1.002	1.000	−0.128	−0.017	
	theo		0.449	11.04	0.959	1.060	−0.100	0.007	0.383
Ni···Ni	exp		0.053	0.68	1.948	1.948	−0.028	0.010	
	theo	3.468	0.139	1.78			−0.101	0.011	0.005

[a]The first line shows experimental values, while the second line provides theoretical values from DFT. The units used are Å for R_{ij} and d, e Å^{-3} for ρ_{bcp}, eÅ^{-5} for $\nabla^2\rho_{bcp}$, and hartree Å^{-3} for V and H.

Another group has also attempted to extract values for the exchange interactions in five compounds from the same cobalt(II) family using magnetometric and magnetooptical data, concluding in their study that all interactions were AFM.[42] Given that all of the M−O−M angles in the compounds measured were greater than 110°, this result lends more weight to the trend observed so far. However, many more compounds would need to be measured before any reliable conclusion could be drawn from such a correlation.

From a magnetic point of view, direct metal−metal bonding is expected to result in a strong AFM interaction. Since both compounds in the present study exhibit FM behavior—however weak—it is unlikely that the there is any significant covalent interaction between the two metals. This is supported by the large distance between the two metals, with M···M distances of 3.505(1) and 3.468(1) Å, respectively, for **1** and **2**. The dominant pathway for the exchange is therefore expected to be along the intervening bonds (superexchange), with the geometry of the bridging water (and by extension, its bonding properties) being a common point of interest.[2,9]

Both the electron density ($\rho = \rho_\alpha + \rho_\beta$) and the spin density ($\rho = \rho_\alpha - \rho_\beta$) depend on the degree of spin−orbit coupling, although the latter significantly more than the former. The spin density can be experimentally probed from flipping ratio measurements using a polarized neutron beam and a magnetized sample,[43] and we are currently performing work in this direction on these compounds, but these results are beyond the scope of this paper and will therefore be published separately. Instead we focus here solely on the ED and the properties that can be derived from this. The intramolecular chemical bonds can be characterized using the topological properties evaluated at the bond critical points (bcps) as shown in Table 3.

Table 3 shows an overall fine agreement between theory and experiment for **1**, but a systematic underestimation of bond strength from DFT when compared to experiment for **2**. Values of ρ_{bcp} increase with decreasing bond length, in accordance with well-known relations for metal−ligand bonds.[44] The M−O bond lengths are on average 0.04 Å longer in **1** than in **2**, while the value of ρ_{bcp} is on average 0.13 e Å^{-3} lower. The total energy density following Abramov's approximation for the kinetic energy density[45] gives positive experimental values for **1**, in agreement with theory. On the other hand, experimental energy densities are negative for **2**, in contrast with the positive theoretical values. Overall, these data suggest a stronger interaction to the bridging water for Ni than for Co, and also indicate a trend of decreasing bond strength, with bridging carboxylate > terminal carboxylate ≈ bridging water > terminal carboxylic acid within a given complex. On average, the Laplacian of the density at the metal−oxygen bcp positions increases nearly linearly with decreasing M−O distance, as shown in Figure 3, and it follows the behavior previously shown to exist for transition metal−oxygen bonds.[44b,46]

The theoretical delocalization index (DI),[47] which provides a measure of bond order, is given in Table 3 for M−O and metal−metal interactions. We note that previous work[48] has shown that the DI can provide a stable and insightful guide to potential metal−metal bonding in 3c−2e bonds, and especially bridged transition metal dimers such as $Co_2(CO)_8$. In ref 48a, the authors quote M−M DI values of between 0.25 and 0.50, depending on the metal and the distance. The metal-to-ligand bonds in **1** and **2** are characterized by δ(M,O) values between 0.3 and 0.5, in accordance with normal bonds of this type, and

dx.doi.org/10.1021/ic501411w | Inorg. Chem. 2014, 53, 11531−11539

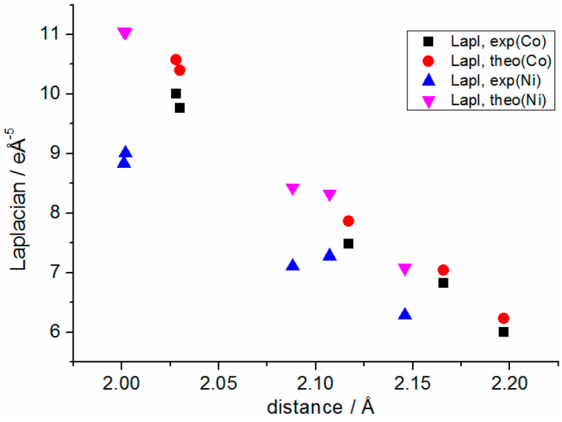

Figure 3. Laplacian of the density from both theory and experiment evaluated at the metal−oxygen bcps.

which also reflect the trend in bond strengths noted above, with the bridging water having a value intermediate between those of carboxylate and carboxylic ligands. In addition, these data provide no evidence for direct metal−metal interaction in either complex, with overlaps between metals exhibiting very small values, in accordance with the large separation and lack of bcp between metals. Moreover, this also agrees with magnetic measurements, since if there indeed was a direct interaction between the atoms, it would be expected to promote strong AFM coupling, and would thus be counter to the experimental results that show weak and likely FM interactions.

It is interesting to compare data for the different SCF solutions. For **1**, the lower-energy broken-symmetry solution was 1.92 eV below the default one, while for **2** this was 3.18 eV lower. Spin density is evident in both complexes (see Supporting Information, Figure S5), but integrated spin charges are close to those found with default solutions (2.739 vs 2.717 in **1**, 0.007 vs 0.000 in **2**). The electron density in M—O bonds is always lower, and the Laplacian of the density uniformly more positive, in the broken-symmetry solutions than in the default ones. Changes in density are relatively constant in **1** (between 6 and 7%), whereas larger changes are found in Ni−O7 (19%) and Ni−O1 (22%) bonds in **2** compared to others (4 to 10%). Similarly, the positive Laplacian in Co−O bonds in **1** is between 10 and 15% greater, whereas that in Ni−O bonds in **2** changes by between 2% (Ni−O1) and 19% (Ni−O5). Overall, the picture of M−O bonding obtained from topological properties changes little between these solutions. However, one striking distance is found in the DI value for **1**, which was 0.709 in the default solution but just 0.005 in the broken-symmetry one (values of 0.006 and 0.005 are found for **2**). Given that all other density properties, experimental and theoretical, as well as magnetic measurements highlight the similarity of **1** and **2**, the identical DI with broken-symmetry solutions suggests that these give a better description of these complexes than the default approach.

To approach the question of bonding between the metal atoms using a nonlocal tool, the source function (SF) has proven useful.[49] It has been shown to be an excellent method for the study of electronic delocalization in conjugated systems,[50] and for enabling a partitioning of the nature of hydrogen bonds from weak to strong low-barrier double wells, to even stronger single-well hydrogen bond values, identified by the change of the hydrogen atomic basin contribution to the H···A bcp.[51] In compounds **1** and **2**, the points of interest are the M−O7 bcp and the M···M midpoint, since these are anticipated to represent the least biased positions concerning the superexchange pathway and the direct exchange, respectively. The values are shown in Table 4. Experimental

Table 4. Integrated Source Function Contributions Given As Percentages for Selected Atomic Basins Evaluated at the Reference Points Corresponding to the M−O7 bcp (columns 2 and 5) and to the M···M Midpoint (columns 3 and 6)

atom[a]	%S(Co−O7)	%S(Co−Co)	atom	%S(Ni−O7)	%S(Ni−Ni)
Co1	31.8	−16.67	Ni1	27.95	−16.90
	25.1	−5.68		26.41	−2.75
O1	−1.59	−5.88	O1	−1.87	−1.48
	−1.04	−3.32		−0.76	−2.35
O2	2.11	5.98	O2	1.32	3.19
	2.13	4.40		1.87	3.44
O3	−2.58	−6.67	O3	−0.53	−2.17
	−0.32	−1.53		−0.10	−1.03
O4	0.70	−0.70	O4	0.96	0.46
	1.23	0.22		1.32	0.60
O5	−0.90	−1.90	O5	0.82	2.09
	0.61	1.31		0.87	0.99
O6	−1.23	−12.43	O6	0.54	−3.15
	0.22	−6.10		0.46	−4.24
O7	36.9	−34.10	O7	35.3	−23.16
	27.0	−4.63		29.1	9.78

[a]For each atom, the first line of data represents experimental values, while the second line represents the theoretical values.

and theoretical values are generally in qualitative agreement, although comparisons are noticeably better at the M−O7 bcp as compared to the M···M midpoint. From experimental data, it is clear that Co and Ni exhibit rather similar distributions, with significant contributions from M and O7 to the M−O7 bond (66% and 63% for Co and Ni, respectively). On the other hand, these two atoms act as sinks to the density at the M···M midpoint (−54% and −40% for Co and Ni, respectively). On the basis of this descriptor, **1** and **2** again appear highly similar. The values of the density at the midpoints between the metal atoms are very small, and the relative errors on the atomic source function contributions at those positions are large.

A link between the magnetism in a cobalt dimer complex, similar to **1**, and the d-orbital populations was recently pointed out by Souhassou et al.[52] In that study, an unexpected rise in the magnetic susceptibility at very low temperatures could be modeled by the introduction of local magnetic anisotropy axes inclined to each other by 37°, and the electron density study faithfully reproduced local d-orbital coordinate systems with the same inclination (in fact the local coordinate systems (LCS) from the density were coinciding with the magnetic axes). In the current family of compounds, there are no discontinuous changes in the magnetic behavior at low temperature despite the complicated magnetic models having to invoke magnetic anisotropy to describe the interactions. Instead, what is observed when comparing different compounds is a (smooth) transition from weak FM to weak AFM intramolecular interactions as the ligand field around the metal atoms is changed (by ligand substitution); the best current description of **1** and **2** is that both are ferromagnetically coupled.

The LCS used to describe the metal d-orbital populations in **1** and **2** was chosen such that the *x*-axis points along the M···M

dx.doi.org/10.1021/ic501411w | Inorg. Chem. 2014, 53, 11531−11539

line and O7 lies in the *xy*-plane. On the basis of this starting point, the most optimal orientation of the local coordinate system was examined by continuous rotation of the LCS using the ERD program.[53] The orientations of the axes that provide the smallest cross terms are not correlated to the cobalt ligand directions, having angular deviations from these directions in excess of 30°, and therefore not adding anything to the understanding of the magnetic behavior in **1** and **2**. Changing the definition of the LCS such that the *z*-axis points to O(7) and with the *x* and *y* axes roughly overlapping with the equatorial M−O/N bonds provides d-orbital populations as shown in Table 5, with the deficit of electrons in the

Table 5. Relative d-Orbital Populations, Given in Percentages of the Total Number of Valence Electrons

compound	d_{z^2}	d_{xz}	d_{yz}	$d_{x^2-y^2}$	d_{xy}	total
1	17.4	24.1	18.9	17.1	22.5	8.23
2	14.7	25.1	26.1	10.1	23.6	7.81

approximate e_g orbitals revealed as the lower populations of $d(z^2)$ and $d(x^2-y^2)$ compared to the other three orbitals. Disregarding covalent contributions, the expected distribution would be 12.5% and 25%. The presence of roughly eight electrons in the valence shell of cobalt—one more than the expected number from a purely ionic picture—and the primary addition of these to the $d(z^2)$ and $d(x^2-y^2)$ orbitals, suggests that significant charge transfer has occurred through covalent interactions with the ligands.

CONCLUSIONS

To summarize, the electron density distributions in two isomorphs of a water-bridged dimetallic carboxylate complex have been determined from a combination of single-crystal X-ray and neutron-diffraction data to obtain anisotropic thermal parameters for the hydrogen atoms. The magnetic properties of other members of this family of compounds have concurrently been thoroughly examined, and it has been shown that the central M−O−M bond angles and the sign of the exchange coupling constant are correlated to some extent. However, the exchange is in all cases weak, and zero-field splitting effects due to orbital contributions overwhelm both the magnetometric and spectroscopic data, leaving some doubt as to the correct nature of the exchange interaction.

In this complementary approach based on the electron density and an atoms-in-molecules partitioning scheme, along with the analysis of delocalization indices and the source function, we see no evidence for direct metal−metal interaction, in accord with the high similarity of the magnetic interactions in the two compounds. This is despite the quite different orbital contributions to the magnetism; in **1**, there is a strong first-order spin−orbit contribution, while **2** has no such first-order contributions but exhibits significant zero-field splitting due to mixing in of excited states.

We are presently performing work on a larger set of compounds derived from this family to examine the influence of ligand type and metal−metal separation on the magnetic properties, as well as further studies highlighting the signatures of magnetic interactions in the electron density. The current study represents the first work in this direction, and indicates that the delocalization index may provide valuable insight into the type and magnitude of magnetic exchange interaction.

ASSOCIATED CONTENT

Supporting Information

Crystallographic information files; residual density analysis, output from comparison of neutron and X-ray derived thermal parameters, additional source function contributions, spin density maps. This material is available free of charge via the Internet at http://pubs.acs.org.

AUTHOR INFORMATION

Corresponding Author

*E-mail: jacobo@chem.au.dk.

Author Contributions

The manuscript was written through contributions of all authors. All authors have given approval to the final version of the manuscript.

Funding

The National Danish Research Council (DNRF93).

Notes

The authors declare no competing financial interest.

ACKNOWLEDGMENTS

We acknowledge the support of the Bragg Institute, Australian Nuclear Science and Technology Organisation, in accepting proposal 2749 for beam time on KOALA. Research conducted at ORNL's Spallation Neutron Source was sponsored by the Scientific User Facilities Division, Office of Basic Energy Sciences, US Department of Energy. J.P.S.W. acknowledges the North West Nanoscience DTC for a Ph.D. studentship. This work was supported by the Danish National Research Foundation (DNRF93) and the Danish Council for Nature and Universe (DanScatt).

REFERENCES

(1) (a) McEvoy, J. P.; Brudvig, G. W. *Chem. Rev.* **2006**, *106*, 4455−4483. (b) Mukhopadhyay, S.; Mandal, S. K.; Bhaduri, S.; Armstrong, W. H. *Chem. Rev.* **2004**, *104*, 3981−4026. (c) Borovik, A. S.; Papaefthymiou, V.; Taylor, L. F.; Anderson, O. P.; Que, L. *J. Am. Chem. Soc.* **1989**, *111*, 6183−6195. (d) Johansson, F. B.; Bond, A. D.; Nielsen, U. G.; Moubaraki, B.; Murray, K. S.; Berry, K. J.; Larrabee, J. A.; McKenzie, C. J. *Inorg. Chem.* **2008**, *47*, 5079−5092. (e) Limburg, J.; Vrettos, J. S.; Liable-Sands, L. M.; Rheingold, A. L.; Crabtree, R. H.; Brudvig, G. W. *Science* **1999**, *283*, 1524−1527.

(2) Boeer, A. B.; Barra, A.-L.; Chibotaru, L. F.; Collison, D.; McInnes, E. J. L.; Mole, R. A.; Simeoni, G. G.; Timco, G. A.; Ungur, L.; Unruh, T.; Winpenny, R. E. P. *Angew. Chem., Int. Ed.* **2011**, *50*, 4007−4011.

(3) Sessoli, R.; Gatteschi, D.; Caneschi, A.; Novak, M. A. *Nature* **1993**, *365*, 141−143.

(4) *Molecular Nanomagnets;* Oxford University Press: New York, 2006; p xii, 395 s., ill.

(5) Crawford, V. H.; Richardson, H. W.; Wasson, J. R.; Hodgson, D. J.; Hatfield, W. E. *Inorg. Chem.* **1976**, *15*, 2107−2110.

(6) (a) Koritsanszky, T. S.; Coppens, P. *Chem. Rev.* **2001**, *101*, 1583−1628. (b) *Modern charge-density analysis;* Springer: New York, 2012.

(7) Bader, R. F. W. *Atoms in molecules;* Oxford University Press: 1990.

(8) Eremenko, I. L.; Golubnichaya, M. A.; Nefedov, S. E.; Sidorov, A. A.; Golovaneva, I. F.; Burkov, V. I.; Ellert, O. G.; Novotortsev, V. M.; Ermenko, L. T.; Sousa, A.; Bermejo, M. R. *Russ. Chem. Bull.* **1998**, *47*, 704−718.

(9) Walsh, J. P. S.; Sproules, S.; Chilton, N. F.; Barra, A.-L.; Timco, G. A.; Collison, D.; McInnes, E. J. L.; Winpenny, R. E. P. *Inorg. Chem.* **2014**, *53*, 8464−8472.

(10) (a) Madsen, A. O.; Sorensen, H. O.; Flensburg, C.; Stewart, R. F.; Larsen, S. *Acta Crystallogr., Sect. A* **2004**, *60*, 550−561. (b) Morgenroth, W.; Overgaard, J.; Clausen, H. F.; Svendsen, H.; Jorgensen, M. R. V.; Larsen, F. K.; Iversen, B. B. *J. Appl. Crystallogr.* **2008**, *41*, 846−853.
(11) Aromí, G.; Batsanov, A. S.; Christian, P.; Helliwell, M.; Parkin, A.; Parsons, S.; Smith, A. A.; Timco, G. A.; Winpenny, R. E. P. *Chem.—Eur. J.* **2003**, *9*, 5142−5161.
(12) Http://www.Ansto.Gov.Au/researchhub/bragg/facilities/instruments/koala/index.Htm (accessed Oct 17, 2014).
(13) Wilkinson, C.; Khamis, H. W.; Stansfield, R. F. D.; McIntyre, G. J. *J. Appl. Crystallogr.* **1988**, *21*, 471−478.
(14) Piltz, R. *Acta Crystallogr., Sect. A* **2011**, *67*, C155.
(15) Jogl, G.; Wang, X.; Mason, S. A.; Kovalevsky, A.; Mustyakimov, M.; Fisher, Z.; Hoffman, C.; Kratky, C.; Langan, P. *Acta Crystallogr., Sect. D* **2011**, *67*, 584−91.
(16) Cosier, J.; Glazer, A. M. *J. Appl. Crystallogr.* **1986**, *19*, 105−107.
(17) Zikovsky, J.; Peterson, P. F.; Wang, X. P. P.; Frost, M.; Hoffmann, C. *J. Appl. Crystallogr.* **2011**, *44*, 418−423.
(18) Schultz, A. J.; Jorgensen, M. R. V.; Wang, X.; Mikkelson, R. L.; Mikkelson, D. J.; Lynch, V. E.; Peterson, P. F.; Green, M. L.; Hoffmann, C. M. *J. Appl. Crystallogr.* **2014**, *47*, 915−921.
(19) Taylor, J.; Arnold, O.; Biheaux, J.; Buts, A.; Campbel, S.; Doucet, M.; Draper, N.; Fowler, R.; Gigg, M.; Lynch, V.; Markvardsen, A.; Palmen, K.; Parker, P.; Peterson, P.; Ren, S.; Reuter, M.; Savici, A.; Taylor, R.; Tolchenov, R.; Whitley, R.; Zhou, W.; Zikovsky, J. *Bull. Am. Phys. Soc.* **2012**, *57*.
(20) Schultz, A. J.; Srinivasan, K.; Teller, R. G.; Williams, J. M.; Lukehart, C. M. *J. Am. Chem. Soc.* **1984**, *106*, 999−1003.
(21) (a) Toby, B. H.; Von Dreele, R. B. *J. Appl. Crystallogr.* **2013**, *46*, 544−549. (b) Toby, B. H. *J. Appl. Crystallogr.* **2001**, *34*, 210−213.
(22) Sheldrick, G. M. *Acta Crystallogr., Sect. A* **2008**, *64*, 112−22.
(23) Dolomanov, O. V.; Bourhis, L. J.; Gildea, R. J.; Howard, J. A. K.; Puschmann, H. *J. Appl. Crystallogr.* **2009**, *42*, 339−341.
(24) *Crysalispro;* Agilent Technologies UK Ltd: Yarnton, England, 2013.
(25) Blessing, R. H. *Acta Crystallogr., Sect. A* **1995**, *51*, 33−38.
(26) Johnson, C. K. *Ortep;* Oak Ridge National Laboratory: Tennessee, U.S., 1965.
(27) Volkov, A.; Macchi, P.; Farrugia, L. J.; Gatti, C.; Mallinson, P.; Richter, T.; Koritsanszky, T. *Xd2006 - a computer program package for multipole refinement, topological analysis of charge densities and evaluation of intermolecular energies from experimental and theoretical structure factors;* 2006.
(28) Hansen, N. K.; Coppens, P. *Acta Crystallogr., Sect. A* **1978**, *34*, 909−921.
(29) Su, Z. W.; Coppens, P. *Acta Crystallogr., Sect. A* **1998**, *54*, 646−652.
(30) Hirshfeld, F. L. *Acta Crystallogr., Sect. A* **1976**, *32*, 239−244.
(31) (a) Meindl, K.; Henn, J. Residual density analysis. In *Electron density and chemical bonding ii: Theoretical charge density studies;* Stalke, D., Ed.; Springer: Berlin, Heidelberg, **2012**; Vol. *147*, pp 143−192;. (b) Meindl, K.; Henn, J. *Acta Crystallogr., Sect. A* **2008**, *64*, 404−418.
(32) Bindzus, N.; Iversen, B. B. *Acta Crystallogr., Sect. A* **2012**, *68*, 750−762.
(33) (a) Overgaard, J.; Jones, C.; Dange, D.; Platts, J. A. *Inorg. Chem.* **2011**, *50*, 8418−8426. (b) Fischer, A.; Tiana, D.; Scherer, W.; Batke, K.; Eickerling, G.; Svendsen, H.; Bindzus, N.; Iversen, B. B. *J. Phys. Chem. A* **2011**, *115*, 13061−13071. (c) Batke, K.; Eickerling, G. *J. Phys. Chem. A* **2013**, *117*, 11566−11579. (d) Koritsanszky, T.; Volkov, A.; Chodkiewicz, M., New directions in pseudoatom-based x-ray charge density analysis. In *Electron density and chemical bonding ii;* Stalke, D., Ed.; Springer: Berlin, Heidelberg, 2012; Vol. *147*, pp 1−25.
(34) Platts, J. A.; Overgaard, J.; Jones, C.; Iversen, B. B.; Stasch, A. *J. Phys. Chem. A* **2011**, *115*, 194−200.
(35) Domagała, S.; Korybut-Daszkiewicz, B.; Straver, L.; Wozniak, K. *Inorg. Chem.* **2009**, *48*, 4010−4020.
(36) Blessing, R. H. *Acta Crystallogr. Sect. B* **1995**, *51*, 816−823.
(37) Jørgensen, M. R. V.; Hathwar, V.; Sist, M.; Wang, X.; Hoffmann, C.; Briseno, A.; Overgaard, J.; Iversen, B. B. *Acta Crystallogr., Sect. A* **2014**, DOI: 10.1107/S2053273314015599.
(38) (a) Becke, A. D. *J. Chem. Phys.* **1993**, *98*, 5648−5652. (b) Lee, C.; Yang, W.; Parr, R. G. *Phys. Rev. B* **1988**, *37*, 785−789.
(39) Weigend, F.; Ahlrichs, R. *Phys. Chem. Chem. Phys.* **2005**, *7*, 3297−3305.
(40) Keith, T. A. *Aimall (version 13.11.04);* TK Gristmill Software: Overland Park, KS, 2013.
(41) Boeer, A. B. *Anisotropy in molecular magnetism—magnetic exchange coupling of octahedral cobalt(II) ions*. Ph.D., The University of Manchester: Manchester, U.K., 2009.
(42) Tomkowicz, Z.; Ostrovsky, S.; Foro, S.; Calvo-Perez, V.; Haase, W. *Inorg. Chem.* **2012**, *51*, 6046−6055.
(43) (a) Papoular, R. J.; Gillon, B. *Europhys. Lett.* **1990**, *13*, 429. (b) Dougan, B. A.; Xue, Z. L. *Sci. China, Ser. B: Chem.* **2009**, *52*, 2083−2095.
(44) (a) Gibbs, G. V.; Ross, N. L.; Cox, D. F.; Rosso, K. M.; Iversen, B. B.; Spackman, M. A. *Phys. Chem. Miner.* **2014**, *41*, 17−25. (b) Gibbs, G. V.; Downs, R. T.; Cox, D. F.; Rosso, K. M.; Ross, N. L.; Kirfel, A.; Lippmann, T.; Morgenroth, W.; Crawford, T. D. *J. Phys. Chem. A* **2008**, *112*, 8811−8823.
(45) Abramov, Y. A. *Acta Crystallogr., Sect. A* **1997**, *53*, 264−272.
(46) (a) Overgaard, J.; Hibbs, D. E.; Rentschler, E.; Timco, G. A.; Larsen, F. K. *Inorg. Chem.* **2003**, *42*, 7593−601. (b) Overgaard, J.; Larsen, F. K.; Schiott, B.; Iversen, B. B. *J. Am. Chem. Soc.* **2003**, *125*, 11088−99.
(47) Fradera, X.; Austen, M. A.; Bader, R. F. W. *J. Phys. Chem. A* **1999**, *103*, 304−314.
(48) (a) Ponec, R.; Gatti, C. *Inorg. Chem.* **2009**, *48*, 11024−11031. (b) Ponec, R.; Uhlik, F. *J. Mol. Struct.: THEOCHEM* **1997**, *391*, 159−168.
(49) Gatti, C.; Lasi, D. *Faraday Discuss.* **2007**, *135*, 55−78.
(50) Monza, E.; Gatti, C.; Lo Presti, L.; Ortoleva, E. *J. Phys. Chem. A* **2011**, *115*, 12864−12878.
(51) Overgaard, J.; Schiott, B.; Larsen, F. K.; Iversen, B. B. *Chem.—Eur. J.* **2001**, *7*, 3756−67.
(52) Deutsch, M.; Claiser, N.; Gillet, J. M.; Lecomte, C.; Sakiyama, H.; Tone, K.; Souhassou, M. *Acta Crystallogr., Sect. B* **2011**, *67*, 324−332.
(53) Sabino, J. R.; Coppens, P. *Acta Crystallogr., Sect. A* **2003**, *59*, 127−131.